ENGINEERING

Standalone real-time health monitoring patch based on a stretchable organic optoelectronic system

Yeongjun Lee[1†], Jong Won Chung[1†], Gae Hwang Lee[1], Hyunbum Kang[1], Joo-Young Kim[1], Chisung Bae[2], Hyunjun Yoo[3], Sujin Jeong[3], Hyeon Cho[3], Sung-Gyu Kang[1], Ji Young Jung[1], Don-Wook Lee[2], Sangah Gam[1], Suk Gyu Hahm[1], Yasutaka Kuzumoto[1], Sang Joon Kim[2], Zhenan Bao[4], Yongtaek Hong[3], Youngjun Yun[1]*, Sunghan Kim[1]

Skin-like health care patches (SHPs) are next-generation health care gadgets that will enable seamless monitoring of biological signals in daily life. Skin-conformable sensors and a stretchable display are critical for the development of standalone SHPs that provide real-time information while alleviating privacy concerns related to wireless data transmission. However, the production of stretchable wearable displays with sufficient pixels to display this information remains challenging. Here, we report a standalone organic SHP that provides real-time heart rate information. The 15-μm-thick SHP comprises a stretchable organic light-emitting diode display and stretchable organic photoplethysmography (PPG) heart rate sensor on all-elastomer substrate and operates stably under 30% strain using a combination of stress relief layers and deformable micro-cracked interconnects that reduce the mechanical stress on the active optoelectronic components. This approach provides a rational strategy for high-resolution stretchable displays, enabling the production of ideal platforms for next-generation wearable health care electronics.

INTRODUCTION

With the growing interest in continuous health monitoring and concerns about public health threats, daily health care platforms are becoming increasingly important (*1*–*3*). Commercial wearables such as smart watches and fitness trackers have proliferated in recent years. Although these devices are widely used for monitoring biological signals, including heart rate, blood oxygen level, and blood pressure, they still struggle to provide accurate physiological information owing to the lack of conformal contact with the skin during daily activities. This has led to the development of electronic skin (e-skin) sensors, which noninvasively detect signals on the skin with conformal contact (*4*–*7*).

Skin-attachable e-skin devices experience various deformational forces due to body movement and thus should be mechanically stretchable (*8*–*10*). Most stretchable electronic devices are rendered mechanically stable via prestraining or geometric engineering approaches, including the use of buckled metal thin films or serpentine metal interconnects (*11*–*14*). Although prestrained buckled structures provide stretchability to flexible materials and devices (*11*, *12*), they are not suitable for high-density optoelectronic device pixel arrays because of pixel overlapping. Moreover, prestraining techniques are not reliable for mass production. Meanwhile, serpentine metal interconnects allow the arrays to be stretched within a certain range depending on their curvature (*13*, *14*). However, the related wavy structures require larger dimensions than those of the active device to achieve high stretchability (*15*, *16*), which hinders the enhancement of pixel resolution. Although emerging stretchable alternating current–driven electroluminescence devices are promising, their operation typically requires high frequency (1 kHz) or a high-voltage (>100 V) source, and they can hardly achieve the required luminance (>10^3 cd/m^2) for outdoor visibility (*17*–*20*). Inorganic micro–light-emitting diodes (micro-LEDs) are also highlighted for flexible and stretchable displays, but there are several challenges to high-yield manufacturing, such as the transfer and bonding of micro-LEDs (*4*). Therefore, a novel approach is required to develop electronic materials and new device architectures of sensors and displays with inherent mechanical stretchability for realizing portable and wireless wearable health care devices.

Here, we report the fabrication of the first organic skin-like health care patch (SHP) by integrating a stretchable organic LED (OLED) array (17 pixels × 7 pixels) with a stretchable organic photoplethysmography (PPG) sensor for real-time measuring and display of the heart rate. The SHP design was optimized by analyzing the strain distribution on the forearm skin by three-dimensional (3D) digital image correlation (DIC) analysis. The stretchable optoelectronic components were fabricated with stress relief layers (SRLs) and stretchable micro-cracked Au interconnects on an all-elastomer substrate (total thickness, ~15 μm), and they could be conformably attached to the skin and operated stably under 30% strain without notable degradation. We believe that the demonstrated standalone device (i.e., a fully integrated system without external devices for power supply or monitoring) would be an ideal platform with high-yield manufacturability that can be commercialized as a wearable e-skin patch for the seamless monitoring of biological information in daily life.

RESULTS

SHP concept and structure

The forearm-mounted SHP detects the PPG waveform at the wrist and displays the measured heart rate (beats per minute) on the OLED matrix display, which is operated by a customized processing module powered by a thin bendable battery (Fig. 1A and fig. S1). An

[1]Organic Material Lab., Samsung Advanced Institute of Technology (SAIT), Samsung Electronics, Suwon 16678, Korea. [2]Computing Platform Lab., Samsung Advanced Institute of Technology (SAIT), Samsung Electronics, Suwon 16678, Korea. [3]Department of Electrical and Computer Engineering, Seoul National University (SNU), Seoul 08826, Korea. [4]Department of Chemical Engineering, Stanford University, Stanford, CA 94305, USA.
*Corresponding author. Email: youngjun.yun@samsung.com
†These authors contributed equally to this work.

Ag epoxy ink connects the processor, OLED array, and PPG sensor, which comprises two red OLEDs and one organic photodiode (OPD) (Fig. 1B). The stretchable optoelectronic components (OLED array and PPG sensor) are located near the wrist, where large strains are induced during wrist movement, while the rigid components (processing module and battery) are placed far from the wrist, where the induced strain is much smaller. Because the wrist has a wide range of motions, the OLED and PPG components are exposed to high mechanical strains. To optimize the SHP design, 3D DIC analysis was used to determine the strain distribution on the forearm during flexion and extension of the wrist (wrist angle, −30° to +60°) (figs. S2 and S3). The strains near the wrist (zone 1) reach 30% at 60° extension, while strains further from the wrist (zone 2, ~6 cm from the wrist) are relatively low, with a maximum strain of <7% (Fig. 1, C and D, and fig. S4). Therefore, the OLED and PPG components must be able to collect high-quality data and display clear information under 30% elongation. The skin-like stretchable SHP was fabricated with a green or red OLED array and conformably attached to a skin replica comprising soft elastomer (Ecoflex rubber) with a Young's modulus (E) comparable to that of human skin (Fig. 1, E and F).

SRLs and deformable interconnects

The stretchable organic optoelectronic components (OLED array and PPG sensor) were fabricated with SRLs and nonwavy metal interconnects. A 17 × 7 array of OLED pixels was used to display clear letters and digits with good readability, as demonstrated on a commercialized smartphone case with a similarly sized LED pixel display (EF-NG930PBEGUS for Samsung Galaxy S7). To optimize the stretchable organic optoelectronic components, we simulated the elongation of the system (ε_{sys}) and deformable electrode ($\varepsilon_{electrode}$) using COMSOL Multiphysics software and calculated the strain distribution ratio as $\sigma = \varepsilon_{electrode} \times \varepsilon_{sys}^{-1}$. The target ε_{sys} (30%) was

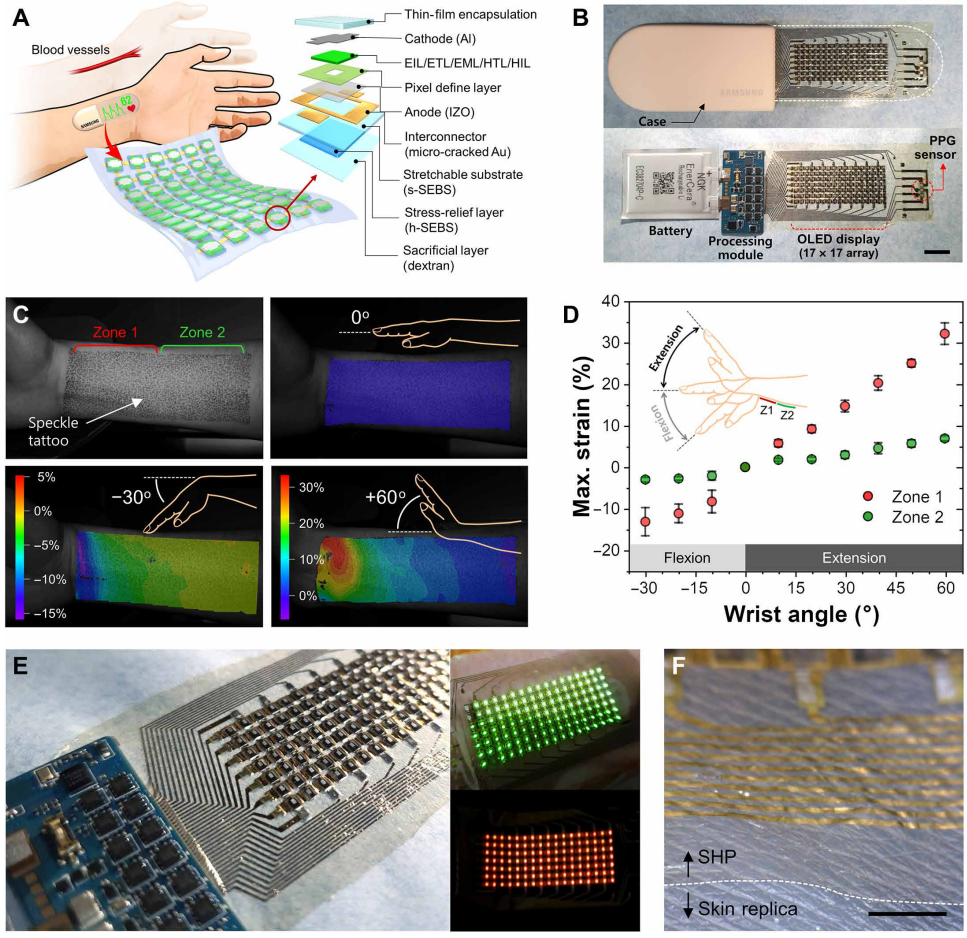

Fig. 1. Concept and structure of a skin-like organic stretchable SHP. (**A**) Schematic of an SHP attached to the forearm to measure the heart rate from the wrist (left) and schematic layout of a single pixel on the SRL-embedded stretchable substrate (right). EIL, electron injection layer; ETL, electron transport layer; EML, emitting layer; HTL, hole transport layer; HIL, hole injection layer; IZO, indium zinc oxide; s- and h-SEBS, soft and hard styrene-ethylene-butylene-styrene, respectively. (**B**) Digital image of a fully integrated standalone SHP comprising an organic stretchable PPG sensor, stretchable OLED display (passive 17 × 7 matrix array), processing module, and thin bendable 3.8-V battery (scale bar, 1 cm). (**C**) Strain mapping image corresponding to skin deformation and strain distribution according to the wrist angle, as obtained by 3D DIC. A random speckle pattern was formed on the forearm (top left), and the strain distribution was analyzed by monitoring the displacement and deformation of the speckles with a change in the wrist angle between −30° and +60°. (**D**) Maximum strain experienced by the skin of the forearm at different wrist angles ranging from −30° to +60°. The forearm area near the wrist (12 cm by 4.5 cm) was divided into two equal parts (area, 6 cm by 4.5 cm) designated as zone 1 (part close to the wrist) and zone 2 (part far from the wrist). (**E**) Digital image of the 15-μm-thick SHP (inset shows green and red OLED arrays). (**F**) Optical micrographs of the SHP conformably attached to a skin replica (scale bar, 250 μm). Photo credit: Yeongjun Lee, SAIT.

achieved by considering the strain distribution on the interconnects ($\varepsilon_{electrode}$) and SRLs. To maximize the pixel size in the stretchable OLED array, we fixed the pixel/interconnect size ratio as 3:1. The maximum strain experienced by the interconnects would be 72 and 116% at 20 and 30% strains, respectively (fig. S5).

Interconnects with low resistivity and small resistance change (R/R_0) under strain are critical for the system. Although the percolation networks of 1D conductive nanomaterials such as carbon nanotubes and Ag nanowires are promising for stretchable electrodes, their low uniformity, high roughness (*21*), and need for solution-coating processes make them unsuitable for high-yield manufacturing and mass production. Further, although vacuum-evaporated metal thin films have low resistivity, uniform surfaces, and reliable film deposition, metal thin films are generally used in the form of either serpentine-structured interconnects or highly sensitive strain sensors owing to their relatively high resistance change [$(R - R_0)/R_0$ of ~35 at 2% strain] (*22*). Moreover, the metal layer can delaminate or crack severely owing to its weak adhesion to the stretchable substrate (*3*).

Metals with low reactivity diffuse into a polymer network during thermal deposition of the Au film near the polymer's glass transition temperature (T_g) (*23*, *24*). In this work, we systematically studied the diffusion of Au into a styrene-ethylene-butylene-styrene (SEBS) block copolymer [styrene/ethylene-butadiene (S/EB) ratio = 20:80, T_g < 80°C] and achieved deformable micro-cracked Au interconnects that are photolithography compatible and do not require structural engineering (e.g., serpentine geometry). Contrary to chemically reactive metals like Al and Cr, inert Au atoms penetrate the surface of the elastomeric polymer and diffuse throughout the free volume during thermal deposition of the Au film. When sufficient Au atoms diffuse into the polymer bulk, Au clusters are formed and anchored in the polymer (Fig. 2A) (*23*).

To achieve deformable Au interconnects (50 nm thick), we evaluated the effect of the Au deposition rate (0.1 to 10 Å/s) (Fig. 2B).

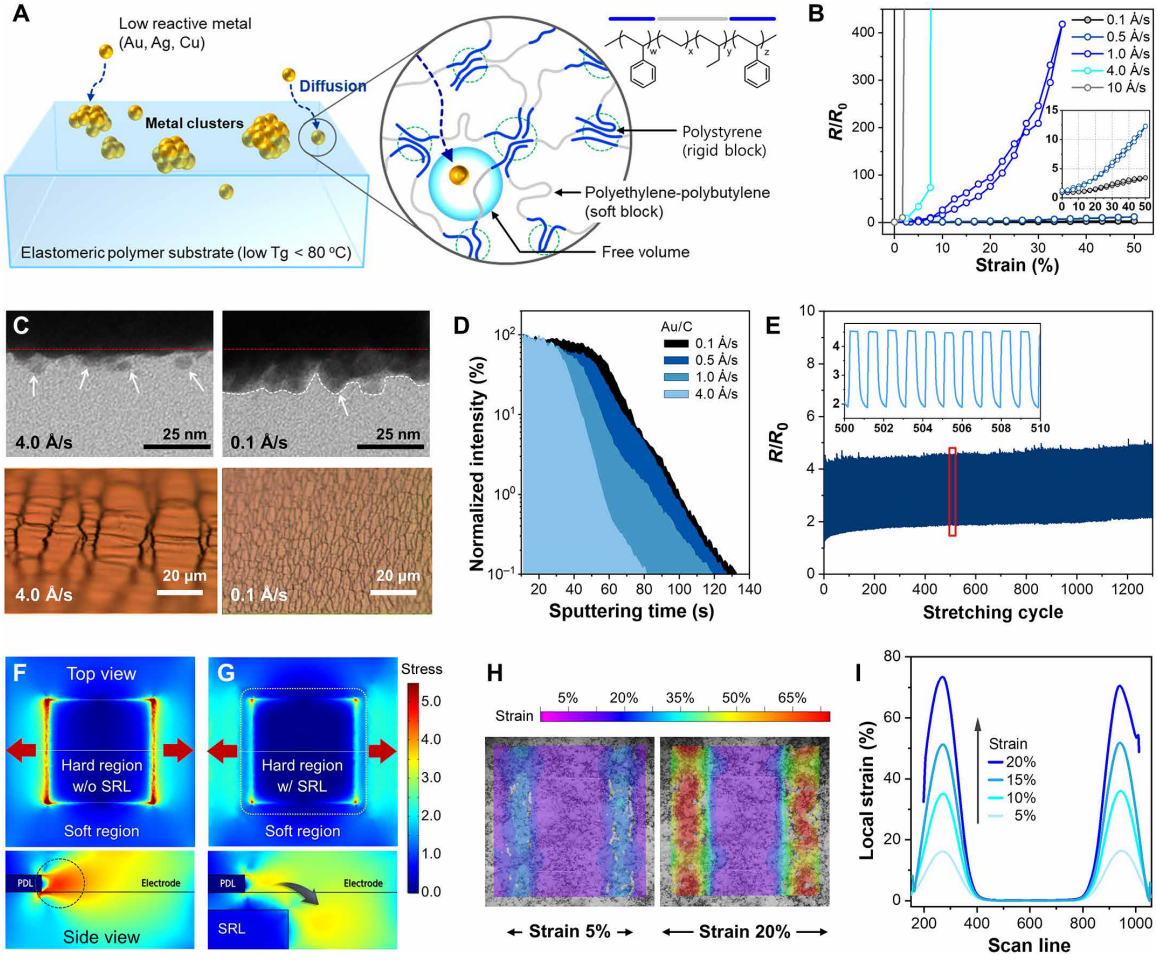

Fig. 2. Fabrication of deformable micro-cracked Au interconnects and SRL. (**A**) Schematic of the formation mechanism of micro-cracked Au interconnects. Au atoms diffused into the elastomer substrate (S/EB ratio = 20:80) during the thermal deposition of the Au film. (**B**) Relative resistance (R/R_0) of the Au electrodes deposited at different rates (0.1 to 10 Å/s) under 0 to 50% strain. (**C**) Focused ion beam–transmission electron microscopy images (top) and optical micrographs (bottom) of Au electrodes deposited at different rates of 4.0 Å/s (left) and 0.1 Å/s (right). (**D**) Secondary ion mass spectrometry depth profile of the Au electrodes deposited at different rates ranging from 0.1 to 4 Å/s. (**E**) Relative resistance (R/R_0) of the Au electrodes over more than 1200 stretching cycles with 30% strain. (**F** and **G**) Simulation of stress distribution at the pixel area on the stretchable substrate with (right) (G) and without (left) (F) the SRL. (**H**) 2D DIC images showing strain distribution on the stretchable substrate with the SRL under 5 and 20% strain. (**I**) Cross-sectional profiles of strain distribution for strains in the range of 0 to 20%.

Because the diffusion of Au atoms follows Fick's second law, and because a certain number of Au atoms is necessary to form Au clusters, more Au atoms entered the SEBS film at a lower deposition rate (0.1 versus 4 Å/s) (Fig. 2C) (*24*). With a deposition rate of 0.1 Å/s, the anchored Au clusters suppress the delamination of the Au film from the polymer surface and the formation of severe cracks [Fig. 2C (bottom) and fig. S6]. We analyzed the Au atom diffusion by secondary ion mass spectrometry and x-ray photoelectron spectroscopy. The Au-to-C peak ratio (Au/C ratio) at different depths reflects the amount of Au atoms that have diffused into the polymer film (Fig. 2D and figs. S7 and S8). In the Au film deposited at 4 Å/s, the normalized intensity of the Au/C ratio decreased sharply with distance, whereas it decreased gradually in the film deposited at 0.1 Å/s. This indicates that more Au atoms diffuse into the polymer film when the Au deposition rate is lower. Moreover, a micro-cracked structure and Au clusters formed at 0.1 Å/s, which maintained the current conduction path under deformation (Fig. 2, B and C). That is, the micro-cracked Au exhibited promising electrical characteristics and stability when deposited at 0.1 Å/s, with a resistivity of 2.67 microhm·m; R/R_0 of 3.43 and 9.03 at 50 and 100% strain, respectively (Fig. 2B and fig. S9); and a stable R/R_0 even after >1200 stretching cycles at 30% strain (Fig. 2E). This demonstrates the potential of this process for producing stretchable interconnects.

The adhesion between the substrate and Au interconnect was examined by a 90° peel test using adhesive tape (Scotch Magic, 3M) attached to a micro-cracked or normal Au interconnect (deposition rate of 0.1 and 10 Å/s, respectively). In contrast to normal Au, which suffered severe damage resulting in a drastic increase in R/R_0 within 10 cycles, the micro-cracked Au remained undamaged and exhibited a stable R/R_0 even after 1000 cycles (fig. S10). Thus, the diffusion of Au atoms into the elastomer increased the adhesion strength.

Next, to minimize the stress on the organic optoelectronic components (OLED array and PPG sensor), an SRL with a higher E than that of the substrate was inserted to modulate the stress distribution on the active components and interconnect regions, thus isolating them from the applied strain. The E of the SEBS copolymer can be adjusted by varying the S/EB ratio. Therefore, soft-SEBS (s-SEBS) (S/EB ratio = 20:80; $E \approx 3.7$ MPa) (*25*) was used as the stretchable substrate, while hard-SEBS (h-SEBS) (S/EB ratio = 67:33; $E \approx 47.3$ MPa) (*26*) was introduced as the SRL. The applied stress is more easily released through s-SEBS owing to its lower E. Notably, the use of soft/hard layers of the same kind of polymer prevented debonding during mechanical deformation (fig. S11). An azide-based ultraviolet (UV) cross-linker was used to improve the chemical resistance of SEBS during the layer-by-layer solution overcoating and subsequent photolithography processes (fig. S12) (*25*).

To optimize the SRL and minimize stress accumulation on the pixel array, we systematically studied the stress distribution on the substrate through mechanical simulation and 2D DIC analysis (Fig. 2, F to I) to predict the optimal thickness ratio of the SRL and substrate (fig. S13). When an active pixel with an E of >119 GPa [e.g., indium zinc oxide (IZO)] is formed on an elastomer substrate (here, s-SEBS with an E of ~3.7 MPa) (*25*, *27*) without the SRL, the applied external stress mainly accumulates near the edge of the rigid pixel area, resulting in mechanical fracture of the interconnects (Fig. 2F). This stress accumulation can be suppressed by introducing an island structure (here, the SRL) with an E of 47.3 MPa. By dispersing the concentrated stress to the edges of the SRL, the strain on the interconnect is reduced (Fig. 2G). We further verified the strain distribution of the stretchable substrate (s-SEBS) with an SRL (h-SEBS) by 2D DIC analysis (Fig. 2H) and found that the strain is distributed in the center of the interconnects rather than accumulating near the edges. At 5, 10, and 20% elongation, the maximum strain on the interconnects was determined to be 16, 35, and 72%, respectively (extrapolated to 106% strain at 30% elongation). The measured strain profile is qualitatively consistent with the simulated one (figs. S5 and S14).

Stretchable OLED/OPD array: Fabrication and characterization

We fabricated an advanced wearable health-monitoring system by leveraging the abovementioned approaches. The overall fabrication process involves layer-by-layer deposition and photolithography for fine patterning (Fig. 3A). The fabrication approach is reliable, scalable, and suitable for mass production and commercialization. A sacrificial layer (dextran, 20 nm) and stretchable substrate (s-SEBS, 5 μm) with patterned SRL (h-SEBS, 5 μm) were deposited onto an 8-inch glass wafer carrier (Fig. 3B) (see Materials and Methods and fig. S15). Then, deformable micro-cracked Au interconnects, the OLED/OPD active device array, and an encapsulation layer were deposited sequentially. IZO transparent anodes (100 nm) and pixel define layers (PDLs; 1.5 μm) with a light-emitting area of 600 μm × 400 μm were photo-patterned on s-SEBS within the h-SEBS regions, followed by the thermal deposition of organic active layers and Al cathode using fine metal masks (see Materials and Methods and fig. S16). To protect the OLEDs from oxygen and moisture and disconnection of the interconnect, which may lead to device degradation, spin coating of poly(tetrafluoroethylene-*co*-2,2,4-trifluoro-5-trifluoromethoxy-1,3-dioxole) [P(TTD-TFE)] (1.5 μm) and atomic layer deposition of Al_2O_3 (100 nm) were conducted to form thin-film encapsulation (TFE) layers. The TFE bilayers were patterned by photolithography to fully cover the entire area of the OLED pixels without extending beyond the SRL (Fig. 3C). The OLED array and PPG sensor were delaminated from the glass wafer carrier, and then Ag epoxy ink was used to connect the OLED display, PPG sensor, and processing module.

The display resolution of the OLED array with an all-elastomer substrate and strain-engineering design was 11 pixels per inch (PPI). Nevertheless, this strategy has the potential to create high-resolution stretchable displays that can compete with the conventional approach that uses a kirigami structure (*28*). Downscaling the pixel size from 508 μm × 508 μm to 127 μm × 127 μm would increase the display resolution from 50 to 200 PPI (fig. S17). We considered the stress accumulation on each pixel after downscaling. In the all-elastomer substrate, the accumulated stress was negligibly changed while reducing the pixel size. However, in a kirigami structure [e.g., polyimide (12.5 μm thick, $E \approx 2$ GPa)/polydimethylsiloxane (20 μm thick, $E \approx$ 1 MPa)], the maximum stress in the interconnects would be much increased due to the increased thickness/pixel size ratio; thereby, the stretchability of the device would be restricted. Therefore, our stretchable platform is a rational strategy for the development of high-resolution stretchable displays.

The fabricated stretchable green OLED display with a 17 × 7 pixel array exhibited stable current and uniform luminance characteristics, comparable to those of a reference device fabricated on a rigid glass substrate (figs. S18 and S19), previously reported high-efficiency flexible OLEDs (*29*, *30*), and previously reported stretchable OLEDs (table S1) (*6*, *11*, *12*, *31*–*37*). There was no noticeable degradation in

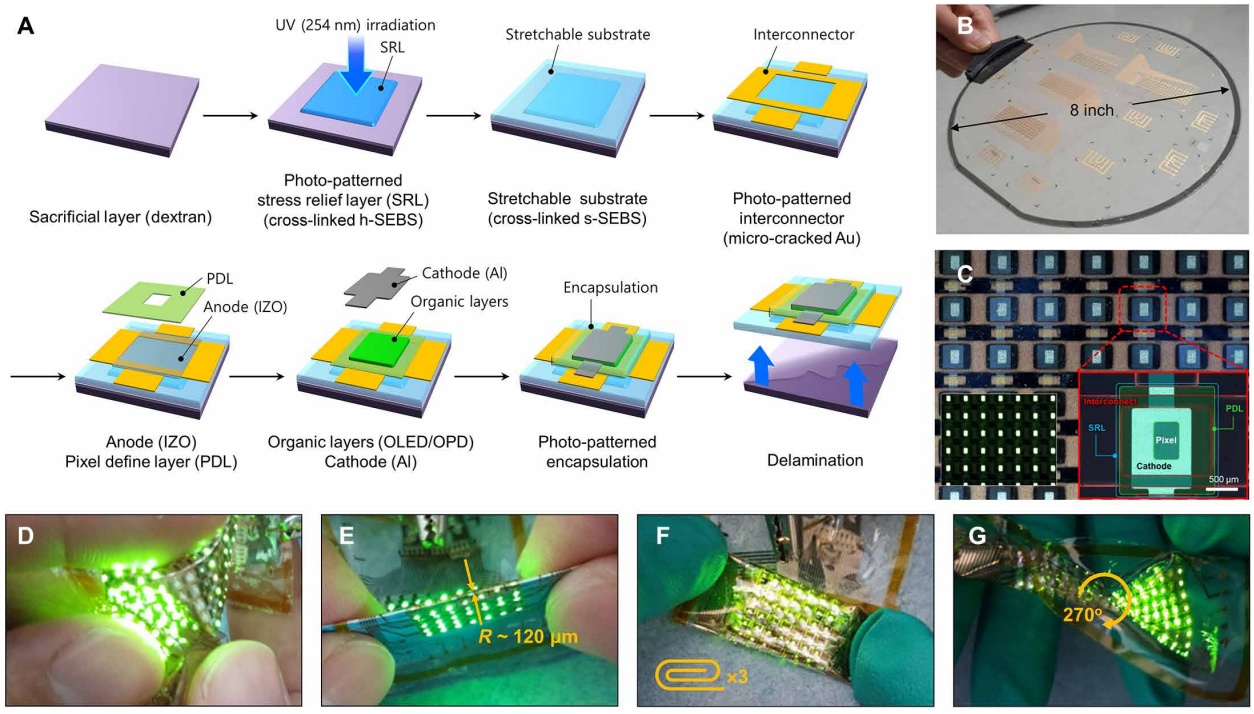

Fig. 3. Fabrication and digital images of the stretchable organic optoelectronic device. (**A**) Overall fabrication process of the stretchable organic optoelectronic device involving layer-by-layer deposition and photolithography. (**B**) Digital image of the stretchable organic optoelectronic device fabricated on an 8-inch glass wafer. (**C**) Microscopic image of a stretchable OLED array. Inset: Electroluminescence image of the stretchable OLED array (left) and magnified view of a single pixel. The image on the right illustrates each layer; the blue, green, and red lines indicate the SRL, PDL, and micro-cracked Au interconnect, respectively. (**D** to **G**) Optical images of the stretchable OLED array under various mechanical deformations: crumpling (D), folding (E), multifolding (F), and twisting (G). Photo credit: Yeongjun Lee, SAIT.

the strain range of 0 to 30% (Fig. 4, A to E, and movie S1) or under various mechanical deformations, including crumpling, folding, and twisting (Fig. 3, D to G, and movie S2). As the deformable micro-cracked Au interconnects were mainly stretched (106% strain under 30% elongation of the OLED array; fig. S14), with the stress accumulation on the OLED pixels minimized by the SRL, the OLED pixels operated stably without any electroluminescence spectral shift or decrease in luminance (Fig. 4, B to F). Further, the increased resistance of the interconnects [initial end-to-end resistance (between pixels 1 and 17) of ~1 kilohm at 0% strain] did not notably change the luminescence of the OLED pixels. Before stretching, the OLED exhibited a luminance of 8510 cd/m^2 with a current density of 10.61 mA/cm^2 at 5.0 V (Fig. 4, D and F). Under 30% strain, the device exhibited a luminance of 8867 cd/m^2 with a current density of 10.72 mA/cm^2. Even after repeated stretching (>1000 cycles) at 25% strain, the OLED maintained a luminance of 8161 cd/m^2 with a current density of 8.78 mA/cm^2. In addition, the current efficiency and quantum efficiency remained constant under strain and after repeated stretching cycles (fig. S19, C and D). Note that the small variation in characteristics originated from the measurement system and not from the device. Because the smallest aperture size (d = 500 μm) of our spectroradiometer is larger than the width of the light-emitting area (w = 400 μm), the aperture was manually focused on the light-emitting area, which might have caused a minor loss in luminance (fig. S18C) (*38*). Therefore, repeated stretching cycles led to a small variation in luminance, but not severe degradation of the device.

To fabricate the stretchable OPD, a transparent IZO anode was deposited and patterned on the SRL. Subsequently, organic layers and Al cathode were vertically stacked sequentially by thermal evaporation through fine metal masks (see Materials and Methods and fig. S20). According to the current density–voltage (J-V) characteristics of the stretchable OPD (Fig. 4F), the dark current density and photocurrent density under illumination (AM 1.5G) are 6.8 × 10^{-7} and 1.74 × 10^{-1} mA/cm^2 at 1 V, respectively. The calculated on/off current density ratio is >2.5 × 10^5, and the external quantum efficiency (EQE) is 39.2% at a wavelength of 625 nm. The detectivity of the stretchable OPD (1.3 × 10^{13} Jones) is comparable to that of a commercial silicon chip–based PD (SFH7060, OSRAM Opto Semiconductors Inc.) (*39*). The stretchable OPD device operated stably under 30% strain (Fig. 4F). In addition, the OPD exhibited a millisecond-scale photo-switching property, which is sufficient to detect real-time dynamic volumetric changes in the blood vessels (Fig. 4G).

The passivation characteristics of TFE bilayer were investigated by measuring the operational lifetime of rigid OLEDs at an initial luminance of 6000 cd/m^2. The T_{95} lifetime (the time for luminance to decline by 95% in air) of an OLED with TFE reached 165 hours. This is comparable to that of a control OLED with conventional glass encapsulation (fig. S21A, closed circles). We also measured the air stability of rigid OPDs with bias stress at −1 V (the operational voltage of the OPD in the PPG sensor), which revealed that the EQE decay of an OPD with TFE was negligible, similar to that of a control OPD with conventional glass encapsulation (fig. S21A, open circles). On the basis of the excellent passivation characteristics of the TFE layers, the stretchable OLED and OPD exhibited a storage lifetime of >15 days in air (fig. S21B).

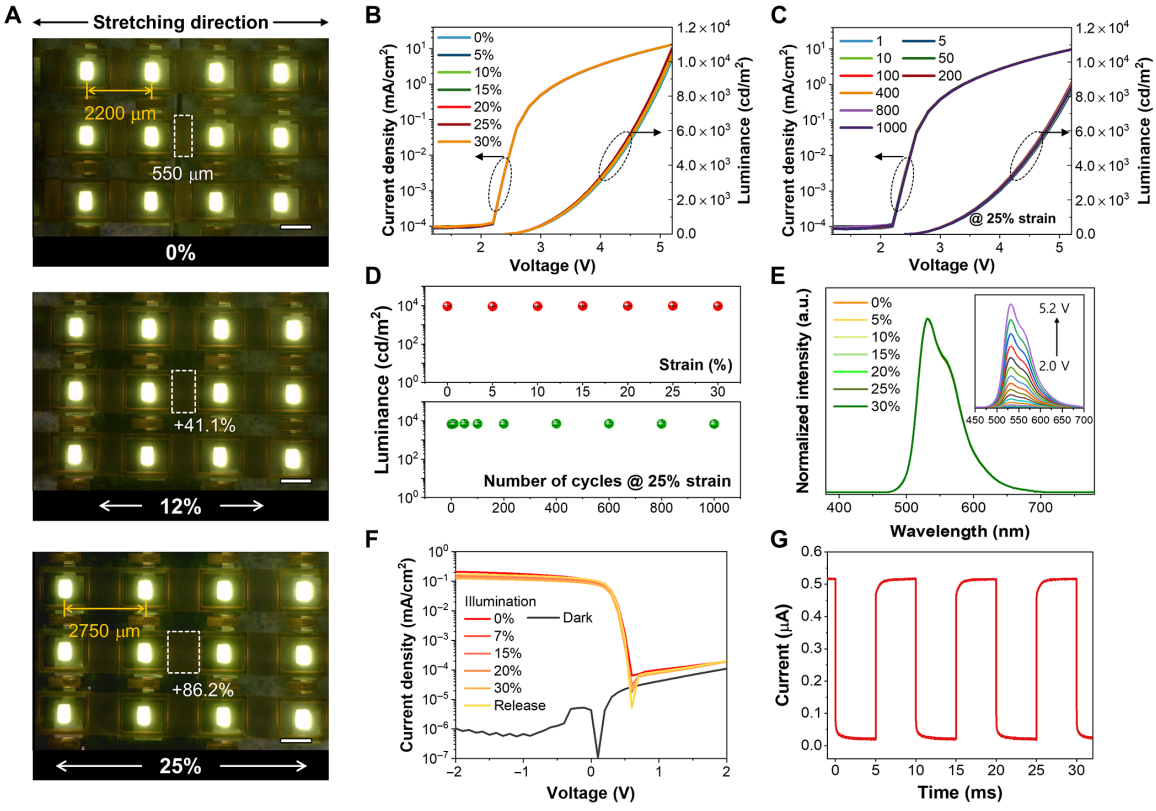

Fig. 4. Characteristics of stretchable OLED and OPD. (**A**) Microscopic images of stretchable OLED pixels under strains of 0, 12, and 25%. The yellow arrows and dashed white boxes indicate the pixel-to-pixel distance and length of the micro-cracked Au interconnect before and after stretching, respectively (scale bar, 1000 μm). The distance between the pixels increased by 25%, while the length of the cracked Au interconnects increased by 86% (dashed white box). (**B** and **C**) Current density–voltage–luminance characteristics of the stretchable OLEDs at strains ranging from 0 to 30% (B) and after stretching cycles at 25% strain (C). (**D**) Variation in the luminance of the stretchable OLED at strains ranging from 0 to 30% (top) and after stretching cycles at 25% strain (bottom). (**E**) Normalized electroluminescence spectra of the stretchable OLED at strains ranging from 0 to 30%. Inset: Electroluminescence spectra of the stretchable OLED at different voltages (2.0 to 5.2 V). a.u., arbitrary units. (**F**) Current density–voltage characteristics of the stretchable OPD under dark and illumination conditions at strains ranging from 0 to 30%. (**G**) Dynamic response of the stretchable OPD.

Real-time heart rate monitoring with SHP on skin

The skin-attachable PPG sensor comprised two red OLEDs and one OPD to achieve a high signal-to-noise ratio based on high brightness (fig. S22). The red light emitted by the OLEDs is reflected by the wrist, and the OPD monitors the variation in the reflected light intensity owing to the volumetric changes in the blood vessels according to the cardiac cycle. The OPD was placed between the two red OLEDs, and the pixel size (1 mm^2) and distance (0.9 mm) were optimized to maximize the signal detection characteristics (Fig. 5A and fig. S22A). The skin-attachable PPG sensor had a high signal-to-noise ratio of >21 dB (fig. S22, C and D), which is comparable to that of a silicon PPG sensor. In addition, the heart rate signal measurement was more robust during wrist movement (repetitive flexion and extension) than that of a silicon PPG sensor (fig. S23) owing to its conformal contact with the wrist, as well as its mechanical stability and high detectivity. The collected signals represent the cardiac cycle waveform with systolic and diastolic peaks (Fig. 5A and fig. S22B).

To obtain a standalone SHP, the stretchable PPG sensor, OLED array, and processing module were powered by a thin bendable 3.8-V Li rechargeable battery (EnerCera, NGK INSULATORS Ltd.) and connected by Ag ink (fig. S24) (*40*). The processing module (Fig. 5B) comprised (i) a microcontroller (nRF52832, Nordic Semiconductor), (ii) voltage regulators (CSD85301Q2T, Texas Instruments) for OLED operation, (iii) a module switch, (iv) boost converters for the OLED/PPG devices, (v) an analog front-end PPG signal processor (AFE4403, Texas Instruments), and (vi) battery connectors.

The processing module is powered by three voltage regulators. A low-dropout linear regulator generates a stable output voltage for the low-power microcontroller and analog front-end PPG. The analog front-end and low-dropout output voltage protect the PPG sensor from deteriorating due to power noise. The stretchable PPG sensor and OLED display are operated by two boost converters. A dot matrix comprising a complementary metal-oxide semiconductor (CMOS) switch array controls the power supply to the rows and columns of OLED array, according to microcontroller output. The analog front-end adjusts the duty cycle of the PPG sensor, reads the signal from the PPG sensor, and transmits it to the microcontroller. The microcontroller filters the raw PPG signals from the analog front-end, extracts the heart rate, and displays the result on the stretchable OLED display. The PPG waveforms detected by the stretchable PPG sensor and analog front-end are digitally filtered by a direct current block filter, low-pass filter [cutoff frequency (f_c) = 0.5 Hz], and high-pass filter (f_c = 10 Hz); then, the heart rate is counted by a peak detection algorithm in the microcontroller. The dot matrix

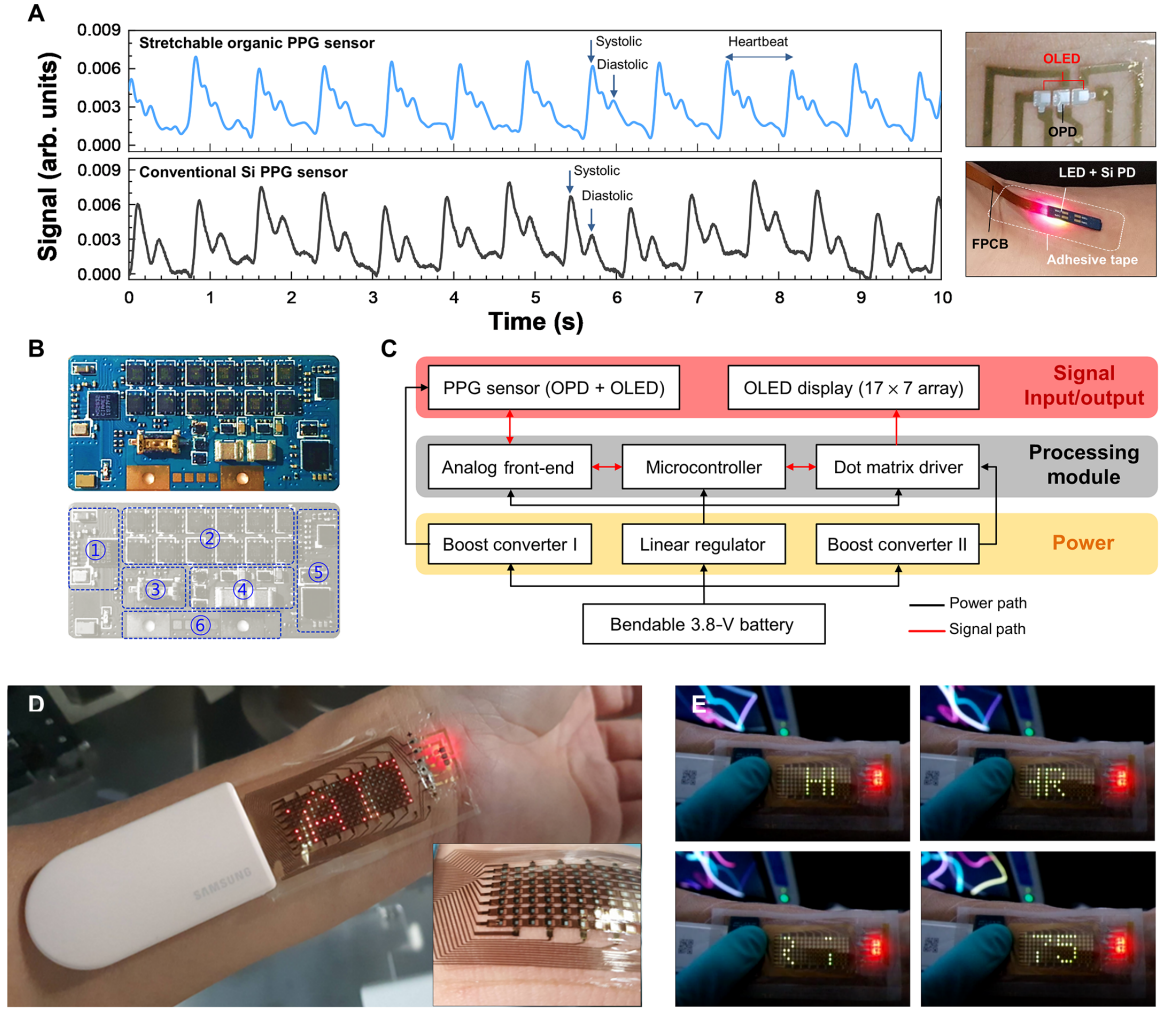

Fig. 5. Standalone skin-like SHP for real-time heart rate monitoring. (**A**) PPG signals measured by a stretchable organic PPG sensor (top) and a conventional silicon chip–based PPG sensor (SFH7060, OSRAM Opto Semiconductors Inc.; bottom) and digital images of each sensor attached on skin. The silicon chip–based PPG sensor is fixed on skin with adhesive tape. (**B**) Photograph of a processing module. The blue box (bottom) illustrates the integrated circuit components of the SHP: (i) microcontroller, (ii) voltage regulators, (iii) module switch, (iv) boost converter, (v) analog front-end, and (vi) battery connectors. (**C**) System block diagram of data transmission from the PPG sensor to OLED display. (**D**) Photographs of the fully integrated standalone SHP device attached on human skin with the red OLED array in dynamic operation (letters "S A I T" are sequentially displayed and scrolled on the OLED array). Inset: SHP on the skin with conformal contact. (**E**) Digital image of the SHP under operation. The heart rate measured by the PPG sensor is displayed in real time on the green OLED array. Photo credit: Yeongjun Lee, SAIT.

driver displays the heart rate on the OLED array in real time (Fig. 5C), with an average power consumption of 16.5 mW.

The OLED pixels in the display have consistent and uniform brightness even when attached to the skin, because the data and scan signals are reliably controlled by the deformable micro-cracked Au interconnects and routers during stretching (movie S3). Last, our fully integrated standalone SHP operated stably when conformably attached to the forearm (Fig. 5D); that is, it measured and displayed the heart rate in real time (Fig. 5E, fig. S25, and movie S4). The letters "HR 75" were displayed and scrolled on the green OLED array, confirming that the measured heart rate is exhibited on the OLED display in real time.

DISCUSSION

In summary, we developed a prototype SHP for the seamless monitoring of biological signals in daily life. By analyzing the strain distribution on the forearm by 3D DIC, we optimized the configuration of the SHP device, comprising stretchable organic optoelectronic components and a battery-operated rigid processing module. The stretchable components (OLEDs and OPDs) were designed by mechanical simulation and 2D DIC to prevent degradation under mechanical strain. The SRL and deformable micro-cracked Au interconnect were developed to efficiently relieve stress accumulation on the pixel area. Our stretchable OLED array can be conformably attached on the human body and stably operated under various mechanical deformations, including crumpling, folding, twisting, and even 30% stretching. As the stretchable OPD provides a high on/off current density ratio of $>2.5 \times 10^5$ and high detectivity of 1.3×10^{13} Jones, the PPG sensor could monitor the pulse wave with a high signal-to-noise ratio of >21 dB. Upon connecting to a thin 3.8-V battery-powered processing module, the SHP could monitor the heart rate in real time. This

stretchable patch fabricated by a reliable and scalable fine-patterning process is a promising platform that could promote the commercialization of wearable electronics for monitoring physical activity, patient management, and smart health tracking. Our SHP is designed to work under 30% elongation, such as that experienced when placed on the wrist. However, when a greater range of elongation is required, we expect that the mechanical stretchability of the device can be further improved by incorporating promising stretchable interconnects based on low-temperature solution processing (*41*–*47*), which have demonstrated excellent electromechanical and stretchable properties. We believe that our SHP, which is the first standalone SHP device, will pave the way for the development of next-generation e-skin health care gadgets, beyond watch- and band-type health trackers.

MATERIALS AND METHODS

Fabrication of a stretchable substrate with SRL

A solution of dextran [Aldrich, 10 weight % (wt %)] in deionized water was spin-coated on an 8-inch glass wafer at 1500 rpm for 20 s. It was then baked on a hot plate at 180°C for 30 min and patterned with a 5-μm-thick SRL. For this, a solution of the elastomer (h-SEBS; Tuftec H1043, Asahi Kasei) and an azide cross-linker [bis(6-((4-azido-2,3,5,6-tetrafluorobenzoyl)oxy)hexyl) decanedioate synthesized according to a method described previously] (*25*) in toluene (Aldrich, 15 wt %) with an h-SEBS/cross-linker ratio of 100:4.5 (w/w) was spin-coated on the dextran film at 500 rpm for 60 s. The deposited film was prebaked at 100°C for 15 min to evaporate the solvent, and then a 100-nm-thick Al layer was thermally deposited on it and patterned by photolithography. The area of the h-SEBS film to be patterned with the Al layer was exposed to 254-nm UV light for 15 min to initiate the photo-crosslinking reaction. Then, the substrate was annealed at 120°C for 15 min on a hot plate in air to increase the degree of cross-linking in the UV-exposed area. Thereafter, the Al layer was removed and the unreacted h-SEBS was removed by rinsing with toluene. Subsequently, the substrate was baked again at 100°C for 15 min to obtain the patterned SRL (h-SEBS) on the dextran layer. After that, a 5-μm-thick s-SEBS film was formed on the SRL and dextran layer, as follows: A solution of s-SEBS (Tuftec H1052, Asahi Kasei) and azide cross-linker (100:3 w/w, 10%) in toluene was spin-coated at 500 rpm for 60 s. The substrate was then prebaked at 100°C for 15 min to evaporate the solvent, and the s-SEBS film was exposed to 254-nm UV light for 15 min to initiate the photo-crosslinking reaction. Subsequently, the substrate was annealed again at 120°C for 15 min on a hot plate in air to increase the degree of cross-linking.

Fabrication and characterization of deformable micro-cracked Au interconnects

A positive photoresist (GXR 601) was patterned on the s-SEBS film using a negative photomask of the router. Then, Au (50 nm thick) was thermally evaporated on the photoresist-patterned substrate at a deposition rate of 0.1 Å/s. The Au atoms selectively diffused into the uncovered s-SEBS surface. Thereafter, another layer of the positive photoresist (GXR 601) was patterned on the Au layer using a positive photomask of the router. Then, the Au layer on the photoresist was etched and the photoresist was stripped to obtain micro-cracked Au interconnects.

Fabrication and characterization of OLED arrays

Stretchable OLED arrays were fabricated on a stretchable substrate with an SRL. An IZO (100 nm) anode layer was sputter-coated on the s-SEBS film and then patterned by photolithography. A PDL (GXR 601, 1.5 μm) patterned by photolithography was placed on the IZO electrode followed by a vertical stack of a hole injection layer [2 wt % Novaled Dopand p-side (Novaled GmbH) (NDP9): *N*-([1,1′-biphenyl]-4-yl)-9,9-dimethyl-*N*-(4-(9-phenyl-9*H*-carbazol-3-yl)phenyl)-9*H*-fluoren-2-amine (BCFA), 10 nm], hole transport layer (HTL; BCFA, 166 nm for green OLED or 206 nm for red OLED), emitting layer (EML; 40 nm), electron transport layer [ETL; Electron Transporter (Novaled GmbH) (NET-164):8-quinolinolato lithium (Liq), 1:1 wt %, 36 nm], electron injection layer (Liq, 5 nm), and cathode (Al, 80 nm) deposited by thermal evaporation with fine metal masks. The OLED pixel was encapsulated by a photo-patterned bilayer comprising P(TTD-TFE) (Hyflon AD, Solvay) (1.5 μm) and Al_2O_3 (100 nm). The current density–voltage–luminance (*J*-*V*-*L*) characteristics and electroluminescence spectra were recorded using a CS2000 spectroradiometer (Konica Minolta Inc.) coupled with a Keithley 2400 parameter analyzer.

OPD fabrication and characterization

An IZO (100 nm) anode layer was sputter-coated on the s-SEBS film and then patterned by photolithography. A PDL (GXR 601, 1.5 μm) patterned by photolithography was placed on the IZO electrode followed by a vertical stack of an HTL (BCFA, 100 nm), layers of subnaphthalocyanines (SubNc, 15 nm), fullerene (C_{60}, 45 nm), bathophenanthroline (BPhen, 10 nm), and Al cathode (80 nm) deposited by thermal evaporation with fine metal masks. The OPD pixel was encapsulated with a photo-patterned bilayer comprising P(TTD-TFE) (1.5 μm) and Al_2O_3 (100 nm). The *J*-*V* characteristics of the OPDs were evaluated using a Keithley 4200 semiconductor parameter analyzer. The EQE spectra were obtained using a spectral photon-to-electron conversion efficiency measurement system under the illumination of monochromatic light generated by an ozone-free Xe lamp equipped with an optical filter (chopper frequency, 30 Hz). The intensity of the incident light was ~0.2 mW/cm^2 at the wavelength of 540 nm.

Operation of the PPG sensor

The PPG sensor was operated with an evaluation module consisting of an integrated analog front-end chip (AFE4490, Texas Instruments). A commercially available reflective PPG sensor (SFH7060, OSRAM Opto Semiconductors Inc.) was used as the reference device.

Dispensing of the Ag epoxy ink

The stretchable PPG sensor, OLED array, and processing module were connected by dispensing Ag epoxy ink (ANP Corp.). Ag patterns with a diameter and thickness of 400 and 150 μm, respectively, were printed on the prepared pads using an automated dispenser (SuperΣ CMIII, Musashi Engineering Inc.). The ink dispensing parameters (e.g., nozzle diameter, 100 μm; pneumatic pressure, 65 kPa; nozzle moving speed, 2 mm/s; nozzle height, 170 μm) were controlled appropriately to obtain uniform patterns of the Ag epoxy ink. The printed Ag patterns were cured by annealing at 180°C for 15 min on a hot plate in air ambient.

Characterization of mechanical stretchability

Stretching tests were conducted using a stretching stage for applying uniaxial tensile strains. Electrical characteristics were evaluated using a Keithley 4200 semiconductor parameter analyzer.

Simulation or mechanical modeling

The commercial COMSOL Multiphysics software based on finite element analysis was used to study mechanics of the stretchable substrate with the SRL. The device layout was optimized to decrease the strain at the edge region of the SRL. The s-SEBS ($E \approx 3.7$ MPa, Poisson's ratio ≈ 0.48) (*25*), h-SEBS ($E \approx 47.3$ MPa, Poisson's ratio ≈ 0.48) (*26*), and stiff IZO ($E \approx 119$ GPa, Poisson's ratio ≈ 0.36) (*27*) were used for the structural modeling. To simplify the analysis, instead of the multiple layers used in the actual OLEDs, we only considered the IZO layer with the highest E in the OLEDs for simulation.

2D and 3D DIC

VIC-2D DIC analysis (Correlated Solutions) was performed with an optical microscope (DSX 510, Olympus). Baking powder (average particle size, ~20 μm) was spread on the stretchable substrate with the SRL mounted on a stretching stage to form 2D speckle patterns. The optical micrographs of the stretched substrate were obtained at 5, 10, 15, and 20% strains. The strain distribution was analyzed using the Hencky (logarithmic) tensor.

The VIC-3D DIC system (Correlated Solutions) consisted of two cameras, which were used for analyzing the strain distribution by the stereo-triangulation method (fig. S2). The two cameras (Schneider Xenoplan 2.0/28 mm Compact Series Lenses) were located 225 mm apart with an angle of 30°. The speckle pattern for the DIC analysis was generated by a program provided by Correlated Solutions with a density of 50%, variation of 75%, and dot diameter of 1 mm. The speckle pattern (fig. S3) was printed on commercially available water transfer tattoo paper (Sunnyscopa). For calibration, 18 calibration images of 9 × 6 dot patterns with a dot size of 7.12 mm and a pitch of 0.89 mm were captured. To capture the skin images, the wrist was placed at 25 cm from the cameras and bent with inward flexion (10° to 40° angle) or outward extension (10° to 60° angle). The images were captured at a 10-Hz frame rate for ~7 s. The strain distribution was analyzed with a Lagrange tensor.

All volunteers confirmed the ethical approval by signing the informed consent before participation in this study. On the basis of the Enforcement Rule of Bioethics and Safety Act, from the Korean Ministry of Health and Welfare, the authors confirm that all experiments performed on human subjects were not subject to local ethics committee approval because there was no invasive measurement or physical modification on human.

SUPPLEMENTARY MATERIALS

Supplementary material for this article is available at http://advances.sciencemag.org/cgi/content/full/7/23/eabg9180/DC1

REFERENCES AND NOTES

1. B. Chu, W. Burnett, J. W. Chung, Z. Bao, Bring on the bodyNET. *Nature* **549**, 328–330 (2017).
2. S. Niu, N. Matsuhisa, L. Beker, J. Li, S. Wang, J. Wang, Y. Jiang, X. Yan, Y. Yun, W. Burnett, A. S. Y. Poon, J. B.-H. Tok, X. Chen, Z. Bao, A wireless body area sensor network based on stretchable passive tags. *Nat. Electron.* **2**, 361–368 (2019).
3. N. Matsuhisa, X. Chen, Z. Bao, T. Someya, Materials and structural designs of stretchable conductors. *Chem. Soc. Rev.* **48**, 2946–2966 (2019).
4. G.-H. Lee, H. Moon, H. Kim, G. H. Lee, W. Kwon, S. Yoo, D. Myung, S. H. Yun, Z. Bao, S. K. Hahn, Multifunctional materials for implantable and wearable photonic healthcare devices. *Nat. Rev. Mater.* **5**, 149–165 (2020).
5. T.-H. Kim, C.-S. Lee, S. Kim, J. Hur, S. Lee, K. W. Shin, Y.-Z. Yoon, M. K. Choi, J. Yang, D.-H. Kim, T. Hyeon, S. Park, S. Hwang, Fully stretchable optoelectronic sensors based on colloidal quantum dots for sensing photoplethysmographic signals. *ACS Nano* **11**, 5992–6003 (2017).
6. T. Yokota, P. Zalar, M. Kaltenbrunner, H. Jinno, N. Matsuhisa, H. Kitanosako, Y. Tachibana, W. Yukita, M. Koizumi, T. Someya, Ultraflexible organic photonic skin. *Sci. Adv.* **2**, e1501856 (2016).
7. H. Lee, E. Kim, Y. Lee, H. Kim, J. Lee, M. Kim, H.-J. Yoo, S. Yoo, Toward all-day wearable health monitoring: An ultralow-power, reflective organic pulse oximetry sensing patch. *Sci. Adv.* **4**, eaas9530 (2018).
8. J. C. Yang, J. Mun, S. Y. Kwon, S. Park, Z. Bao, S. Park, Electronic skin: Recent progress and future prospects for skin-attachable devices for health monitoring, robotics, and prosthetics. *Adv. Mater.* **31**, 1904765 (2019).
9. J. Y. Oh, Z. Bao, Second skin enabled by advanced electronics. *Adv. Sci.* **6**, 1900186 (2019).
10. I. You, D. G. Mackanic, N. Matsuhisa, J. Kang, J. Kwon, L. Beker, J. Mun, W. Suh, T. Y. Kim, J. B.-H. Tok, Z. Bao, U. Jeong, Artificial multimodal receptors based on ion relaxation dynamics. *Science* **370**, 961–965 (2020).
11. M. S. White, M. Kaltenbrunner, E. D. Głowacki, K. Gutnichenko, G. Kettlgruber, I. Graz, S. Aazou, C. Ulbricht, D. A. M. Egbe, M. C. Miron, Z. Major, M. C. Scharber, T. Sekitani, T. Someya, S. Bauer, N. S. Sariciftci, Ultrathin, highly flexible and stretchable PLEDs. *Nat. Photon.* **7**, 811–816 (2013).
12. S. Jeong, H. Yoon, B. Lee, S. Lee, Y. Hong, Distortion-free stretchable light-emitting diodes via imperceptible microwrinkles. *Adv. Mater. Technol.* **5**, 2000231 (2020).
13. J. A. Fan, W.-H. Yeo, Y. Su, Y. Hattori, W. Lee, S.-Y. Jung, Y. Zhang, Z. Liu, H. Cheng, L. Falgout, M. Bajema, T. Coleman, D. Gregoire, R. J. Larsen, Y. Huang, J. A. Rogers, Fractal design concepts for stretchable electronics. *Nat. Commun.* **5**, 3266 (2014).
14. T. Pan, M. Pharr, Y. Ma, R. Ning, Z. Yan, R. Xu, X. Feng, Y. Huang, J. A. Rogers, Experimental and theoretical studies of serpentine interconnects on ultrathin elastomers for stretchable electronics. *Adv. Funct. Mater.* **27**, 1702589 (2017).
15. X. Hu, P. Krull, B. de Graff, K. Dowling, J. A. Rogers, W. J. Arora, Stretchable inorganic-semiconductor electronic systems. *Adv. Mater.* **23**, 2933–2936 (2011).
16. D. Kim, G. Shin, Y. J. Kang, W. Kim, J. S. Ha, Fabrication of a stretchable solid-state micro-supercapacitor array. *ACS Nano* **7**, 7975–7982 (2013).
17. D. Son, J. Kang, O. Vardoulis, Y. Kim, N. Matsuhisa, J. Y. Oh, J. W. F. To, J. Mun, T. Katsumata, Y. Liu, A. F. McGuire, M. Krason, F. Molina-Lopez, J. Ham, U. Kraft, Y. Lee, Y. Yun, J. B.-H. Tok, Z. Bao, An integrated self-healable electronic skin system fabricated via dynamic reconstruction of a nanostructured conducting network. *Nat. Nanotechnol.* **13**, 1057–1065 (2018).
18. D. W. Kim, G. Lee, M. Pal, U. Jeong, Highly deformable transparent Au film electrodes and their uses in deformable displays. *ACS Appl. Mater. Interfaces* **12**, 41969–41980 (2020).
19. H. Zhou, J. Park, Y. Lee, J.-M. Park, J.-H. Kim, J. S. Kim, H.-D. Lee, S. H. Jo, X. Cai, L. Li, X. Sheng, H. J. Yun, J.-W. Park, J.-Y. Sun, T.-W. Lee, Water passivation of perovskite nanocrystals enables air-stable intrinsically stretchable color-conversion layers for stretchable displays. *Adv. Mater.* **32**, 2001989 (2020).
20. G. Lee, M. Kong, D. Park, J. Park, U. Jeong, Electro-photoluminescence color change for deformable visual encryption. *Adv. Mater.* **32**, 1907477 (2020).
21. J. Park, I. You, T. Y. Kim, J. Song, U. Jeong, Ag nanowire-based transparent stretchable tactile sensor recognizing strain directions and pressure. *Nanotechnology* **30**, 315502 (2019).
22. D. Kang, P. V. Pikhitsa, Y. W. Choi, C. Lee, S. S. Shin, L. Piao, B. Park, K.-Y. Suh, T.-i. Kim, M. Choi, Ultrasensitive mechanical crack-based sensor inspired by the spider sensory system. *Nature* **516**, 222–226 (2014).
23. F. Faupel, R. Willecke, A. Thran, Diffusion of metals in polymers. *Mater. Sci. Eng. R* **22**, 1–55 (1998).
24. F. Faupel, A. Thran, M. Kiene, T. Strunskus, V. Zaporojtchenko, K. Behnke, Diffusion of metals in polymers and during metal/polymer interface formation, in *Low Dielectric Constant Materials for IC Applications*, P. S. Ho, J. J. Leu, W. W. Lee, Eds. (Springer, 2003), pp. 221–251.
25. S. Wang, J. Xu, W. Wang, G.-J. N. Wang, R. Rastak, F. Molina-Lopez, J. W. Chung, S. Niu, V. R. Feig, J. Lopez, T. Lei, S.-K. Kwon, Y. Kim, A. M. Foudeh, A. Ehrlich, A. Gasperini, Y. Yun, B. Murmann, J. B.-H. Tok, Z. Bao, Skin electronics from scalable fabrication of an intrinsically stretchable transistor array. *Nature* **555**, 83–88 (2018).
26. W. Wang, S. Wang, R. Rastak, Y. Ochiai, S. Niu, Y. Jiang, P. K. Arunachala, Y. Zheng, J. Xu, N. Matsuhisa, X. Yan, S.-K. Kwon, M. Miyakawa, Z. Zhang, R. Ning, A. M. Foudeh, Y. Yun, C. Linder, J. B.-H. Tok, Z. Bao, Strain-insensitive intrinsically stretchable transistors and circuits. *Nat. Electron.* **4**, 143–150 (2021).
27. S. Park, K. Cho, H. Oh, S. Kim, Electrical and mechanical characteristics of fully transparent IZO thin-film transistors on stress-relieving bendable substrates. *Appl. Phys. Lett.* **109**, 143504 (2016).
28. J. M. Shin, S. Kim, G. Lee, H. Joo, J. Hong, Display module. U.S. Patent 20200312248.
29. S.-H. Jeong, S.-H. Woo, T.-H. Han, M.-H. Park, H. Cho, Y.-H. Kim, H. Cho, H. Kim, S. Yoo, T.-W. Lee, Universal high work function flexible anode for simplified ITO-free organic and perovskite light-emitting diodes with ultra-high efficiency. *NPG Asia Mater.* **9**, e411 (2017).
30. S. Ahn, T.-H. Han, K. Maleski, J. Song, Y.-H. Kim, M.-H. Park, H. Zhou, S. Yoo, Y. Gogotsi, T.-W. Lee, A 2D titanium carbide MXene flexible electrode for high-efficiency light-emitting diodes. *Adv. Mater.* **32**, 2000919 (2020).

31. M. S. Lim, M. Nam, S. Choi, Y. Jeon, Y. H. Son, S.-M. Lee, K. C. Choi, Two-dimensionally stretchable organic light-emitting diode with elastic pillar arrays for stress relief. *Nano Lett.* **20**, 1526–1535 (2020).
32. J.-H. Hong, J. M. Shin, G. M. Kim, H. Joo, G. S. Park, I. B. Hwang, M. W. Kim, W.-S. Park, H. Y. Chu, S. Kim, 9.1-inch stretchable AMOLED display based on LTPS technology. *J. Soc. Inf. Disp.* **25**, 194–199 (2017).
33. Z. Yu, X. Niu, Z. Liu, Q. Pei, Intrinsically stretchable polymer light-emitting devices using carbon nanotube-polymer composite electrodes. *Adv. Mater.* **23**, 3989–3994 (2011).
34. J. Liang, L. Li, X. Niu, Z. Yu, Q. Pei, Elastomeric polymer light-emitting devices and displays. *Nat. Photon.* **7**, 817–824 (2013).
35. J. Liang, L. Li, K. Tong, Z. Ren, W. Hu, X. Niu, Y. Chen, Q. Pei, Silver nanowire percolation network soldered with graphene oxide at room temperature and its application for fully stretchable polymer light-emitting diodes. *ACS Nano* **8**, 1590–1600 (2014).
36. D. Yin, J. Feng, R. Ma, Y.-F. Liu, Y.-L. Zhang, X.-L. Zhang, Y.-G. Bi, Q.-D. Chen, H.-B. Sun, Efficient and mechanically robust stretchable organic light-emitting devices by a laser-programmable buckling process. *Nat. Commun.* **7**, 11573 (2016).
37. D. Yin, N.-R. Jiang, Y.-F. Liu, X.-L. Zhang, A.-W. Li, J. Feng, H.-B. Sun, Mechanically robust stretchable organic optoelectronic devices built using a simple and universal stencil-pattern transferring technology. *Light Sci. Appl.* **7**, 35 (2018).
38. S.-H. Jeong, J. Park, T.-H. Han, F. Zhang, K. Zhu, J. S. Kim, M.-H. Park, M. O. Reese, S. Yoo, T.-W. Lee, Characterizing the efficiency of perovskite solar cells and light-emitting diodes. *Joule* **4**, 1206–1235 (2020).
39. I. K. Kim, J. H. Jo, J. Lee, Y. J. Choi, Detectivity analysis for organic photodetectors. *Org. Electron.* **57**, 89–92 (2018).
40. J. Byun, B. Lee, E. Oh, H. Kim, S. Kim, S. Lee, Y. Hong, Fully printable, strain-engineered electronic wrap for customizable soft electronics. *Sci. Rep.* **7**, 45328 (2017).
41. L. Zhang, H. Ji, H. Huang, N. Yi, X. Shi, S. Xie, Y. Li, Z. Ye, P. Feng, T. Lin, X. Liu, X. Leng, M. Li, J. Zhang, X. Ma, P. He, W. Zhao, H. Cheng, Wearable circuits sintered at room temperature directly on the skin surface for health monitoring. *ACS Appl. Mater. Interfaces* **12**, 45504–45515 (2020).
42. M. Amit, R. K. Mishra, Q. Hoang, A. M. Galan, J. Wang, T. N. Ng, Point-of-use robotic sensors for simultaneous pressure detection and chemical analysis. *Mater. Horiz.* **6**, 604–611 (2019).
43. N. Matsuhisa, D. Inoue, P. Zalar, H. Jin, Y. Matsuba, A. Itoh, T. Yokota, D. Hashizume, T. Someya, Printable elastic conductors by *in situ* formation of silver nanoparticles from silver flakes. *Nat. Mater.* **16**, 834–840 (2017).
44. S. Choi, S. I. Han, D. Jung, H. J. Hwang, C. Lim, S. Bae, O. K. Park, C. M. Tschabrunn, M. Lee, S. Y. Bae, J. W. Yu, J. H. Ryu, S.-W. Lee, K. Park, P. M. Kang, W. B. Lee, R. Nezafat, T. Hyeon, D.-H. Kim, Highly conductive, stretchable and biocompatible Ag–Au core–sheath nanowire composite for wearable and implantable bioelectronics. *Nat. Nanotechnol.* **13**, 1048–1056 (2018).
45. S. Veerapandian, W. Jang, J. B. Seol, H. Wang, M. Kong, K. Thiyagarajan, J. Kwak, G. Park, G. Lee, W. Suh, I. You, M. E. Kılıç, A. Giri, L. Beccai, A. Soon, U. Jeong, Hydrogen-doped viscoplastic liquid metal microparticles for stretchable printed metal lines. *Nat. Mater.* **20**, 533–540 (2021).
46. Y. Wang, C. Zhu, R. Pfattner, H. Yan, L. Jin, S. Chen, F. Molina-Lopez, F. Lissel, J. Liu, N. I. Rabiah, Z. Chen, J. W. Chung, C. Linder, M. F. Toney, B. Murmann, Z. Bao, A highly stretchable, transparent, and conductive polymer. *Sci. Adv.* **3**, e1602076 (2017).
47. K. N. Al-Milaji, Q. Huang, Z. Li, T. N. Ng, H. Zhao, Direct embedment and alignment of silver nanowires by inkjet printing for stretchable conductors. *ACS Appl. Mater. Interfaces* **2**, 3289–3298 (2020).
48. M. V. Hoang, H.-J. Chung, A. L. Elias, Irreversible bonding of polyimide and polydimethylsiloxane (PDMS) based on a thiol-epoxy click reaction. *J. Micromech. Microeng.* **26**, 105019 (2016).

Acknowledgments

Author contributions: Y.L., J.W.C., and Y.Y. conceived and designed the experiments. G.H.L. carried out the mechanical simulation. Y.Y. designed the OLED and PPG circuit. Y.L., J.W.C., G.H.L., H.K., J.-Y.K., S.-G.K., J.Y.J., D.-W.L., S.G., S.G.H., and Y.K. conducted investigations, verification, and data curation. C.B. and S.J.K. designed and developed the processing module. H.Y., S.J., and H.C. conducted 2D and 3D DIC data analysis. Z.B. and Y.H. contributed to the analysis and discussion of results. Y.Y. and S.K. supervised the project. Y.L. and J.W.C. organized the data and wrote the manuscript. All the authors contributed to the reviewing and editing of the manuscript at all stages. **Competing interests:** Y.L., H.K., G.H.L., J.W.C., J.-Y.K., S.G.H., and Y.Y. are inventors on patent applications related to this work filed by Samsung Electronics Co. Ltd. (KR 10-2020-0093154, 27 July 2020; KR 10-2020-0098177, 5 August 2020; KR 10-2020-0124014, 24 September 2020). The authors declare no other competing interests. **Data and materials availability:** All data needed to evaluate the conclusions in the paper are present in the paper and/or the Supplementary Materials. Additional data related to this paper may be requested from the authors.

Submitted 4 February 2021
Accepted 19 April 2021
Published 4 June 2021
10.1126/sciadv.abg9180

Citation: Y. Lee, J. W. Chung, G. H. Lee, H. Kang, J.-Y. Kim, C. Bae, H. Yoo, S. Jeong, H. Cho, S.-G. Kang, J. Y. Jung, D.-W. Lee, S. Gam, S. G. Hahm, Y. Kuzumoto, S. J. Kim, Z. Bao, Y. Hong, Y. Yun, S. Kim, Standalone real-time health monitoring patch based on a stretchable organic optoelectronic system. *Sci. Adv.* **7**, eabg9180 (2021).